Ultrafast x-ray processes with hollow atoms

Kengo Moribayashi,[1] Akira Sasaki,[1] and T. Tajima[1,2]
[1]*Advanced Photon Research Center, Japan Atomic Energy Research Institute, 25-1, Mii-minami-cho, Neyagawa-shi, Osaka 572, Japan*
[2]*Department of Physics and Institute for Fusion Studies, University of Texas at Austin, Austin, Texas 78712*
(Received 24 March 1998)

An ultrafast inner-shell ionization process, together with x-ray emission stimulated by high-intensity short-pulse x rays, is studied. In this process it is found that the multi-inner-shell ionization predominates, leading to the formation of hollow atoms. These hollow atoms play an instrumental role in high brightness x-ray measurements of the ultrafast dynamics in chemistry, biochemistry, biology, and materials. As the pumping x-ray power and thus the density of hollow atoms are increased, the emission of x rays is not only of significance for the measurement but is good for x-ray lasing. This lasing mechanism has a clear advantage over the conventional inner-shell ionization method, yielding a gain value of more than 10^4 cm^{-1} over a relatively long time. Classes of experiments of pump x-ray probe and x-ray laser are suggested. [S1050-2947(98)01009-9]

PACS number(s): 32.80.Hd, 42.55.Vc, 52.25.Nr

I. INTRODUCTION

The emission of high-intensity short-pulse x rays [1–5] has attracted a great deal of attention, stimulated by a remarkable advance in short-pulse laser technology [6–9]. In the present paper we show an example of the production of x rays with the use of the interaction of atoms with high-intensity short-pulse x rays. We find that an ultrafast atomic process resulting from this interaction can give rise to the formation of hollow atoms. Further, it is found that this formation has favorable properties for x-ray laser emission. It may be also useful for high-brightness x-ray measurement.

Recent progress in intense pulsed lasers allows new sources of high-power x rays such as high harmonic generation [1], which is based on laser driven periodic bremsstrahlung. Among these x-ray processes upon the irradiation of intense laser pulses on low-Z matter the Larmor radiation due to the acceleration of electrons in the laser electromagnetic fields is of much importance for the drive of ultrafast optical processes involving the inner-shell excitation. This Larmor radiation driven by intense short laser pulses has the following properties. (1) The radiative spectrum of Larmor x rays has a peak at $\omega = a_0^3 \omega_0$ [where ω_0 and a_0 are the laser frequency and normalized laser field $(a_0 = eE_0/m\omega_0 c)$], in contrast to the bremsstrahlung whose spectrum is flat. Only when the laser power enters the relativistic regime ($a_0 \geqslant 1$), does the laser-induced Larmor x ray begin to appear. (2) The radiative power of Larmor radiation increases linearly proportional to the laser intensity and to the density of electrons, whereas the bremsstrahlung power increases in proportion to 1.5 powers of the laser intensity and square of the electron density. Although many nonlinear processes can change, the linear intensity of Larmor radiation is [5]

$$I_{LX}(\mathrm{W/cm^2}) \sim 0.91 \times 10^{15} a_0^2 \frac{a_0^2+8}{2a_0^2+8} \left(\frac{1\ \mu\mathrm{m}}{\lambda_L} \right)^2 \times \left(\frac{n_e}{10^{21}\ \mathrm{cm^{-3}}} \right) Z_R , \quad (1)$$

where n_e, λ_L, and Z_R are the electron density, laser wavelength, and propagation length. (3) The x-ray power bursts in a very sharp and short pulse (comparable to the laser pulse length). For example, at the laser power of 30 TW focused on a 3-μm×10-μm target, the x-ray intensity due to the Larmor is 10^{16} W/cm^2 and the peak energy is about 200 eV by setting up the parameter values of $a_0 = 6$, $\lambda_L = 1\ \mu$m, $n_e = 3 \times 10^{22}$ cm^{-3}, and $Z_R = 100\ \mu$m. Alternative methods to the Larmor x rays to obtain the driving x rays may be x rays generated by surface high-energy electrons [10] or x rays by inner-shell electron bremsstrahlung of a high Z material driven by intense laser. Irradiating such x rays on certain atoms with appropriate conditions should lead to ultrafast inner-shell excitation.

As Guo *et al.* have pointed out in their experimental demonstration of the lattice displacement of GaAs single crystals [11], pump x-ray probe techniques with the use of such high-intensity short-pulse x-ray sources are essential in developing the measurement of ultrafast processes in chemistry, biochemistry, biology, and material science. (They measured it at intervals of a few picoseconds.) In femtosecond spectroscopy, pump-probe techniques together with the advance of femtosecond-pulse laser technology enable us to realize the measurement of the femtosecond ultrafast chemical reaction [12]. Further, this method has given birth to the detection of some remarkable new ultrafast processes in biology, for example in the photoreceptors of our eyes [13–15], or photosynthesis [16–18]. We believe that pump x-ray probe techniques by the high-brightness femtosecond-pulse x-ray sources resulting from Larmor radiation are very useful for the understanding of femtosecond processes. Namely, we can measure the components, states, and structures of femtosecond processes in chemistry and biology. We show a class of the experiment of high-intensity femtosecond-pulse x-ray measurement. Moreover, hollow atoms as well as inner-shell excited states may play an important role in such high-brightness x-ray measurements. The detection of the x-ray emission from hollow atoms [19–21], which results from the interaction between a slow ion with a few electrons and the surface, is also a noteworthy topic.

The inner-shell ionization process has been thought to be among the useful methods for x-ray laser emission [22–27].

It was proposed by Duguay and Rentzepis [22]. However, there is no experimental demonstration of this method for the x-ray laser emission as far as we know. Kapteyn [24] and Moon *et al.* [25] theoretically showed that the lasing gain of $10\ \mathrm{cm}^{-1}$ in the ''water window'' frequency regime associated with the $K\alpha$ transitions is possible by irradiating x rays of 10^{14}–10^{15} W/cm^2 intensity and 50 fs duration on Ne or C atoms with 10^{20}-cm^{-3} density. Because of secondary electron-impact ionization it has been thought [23] that a low density ($\leqslant 10^{20}\ \mathrm{cm}^{-3}$) is needed for operation, which of course amounts to a (relatively) low gain. In our previous paper [27] we showed that the formation of hollow atoms contributes to overcoming this detrimental effect of the secondary electron impact ionization by taking an example of the Na atoms with no $2p$ electrons. Further we pointed out that the $3s\rightarrow 2p$ transitions (in comparison to the $K\alpha$ transitions of C) of low Z atoms reduce the necessary intensity of the x-ray source. Thus, we employ the $3s\rightarrow 2p$ transition of Na as the atomic process, as the Na atom is the simplest for an x-ray laser with the $3s\rightarrow 2p$ transition. [For example, the inner-shell $2p$ electron excited states in Na cannot decay through autoionization (Auger) processes.] Among the possibilities such as a NaH molecular crystal or nonmetallic vapor Na less than one-sixth of the solid density [28], we adopt a NaH crystal. In hollow atoms with no $2p$ electrons of a Na atom, the $3s$ electron of NaH may be treated as an atomic state: the attractive force from the Na atomic nucleus is much stronger than that from hydrogen because there is no screening effect by $2p$ electrons of the Na atom. (We may ignore atomic processes in the H atom because the photoionization cross sections of H are much smaller than those of the Na atom with the use of the photon with 50–500 eV [29].) In this paper, we show more detailed results. Further we calculate the x-ray laser from the hollow atoms with no $1s$ electrons of the C atoms in order to show that the hollow atoms of the NaH crystal have a clear advantage as mentioned before. We consider ultrafast atomic processes in the generation of hollow atoms and associated x-ray emission with the use of a high-intensity short-pulse x-ray pumping source. We model a system of NaH crystal and that of solid C at a density of $\sim 10^{22}\ \mathrm{cm}^{-3}$ to derive the analytical solution of the populations and to find the condition for x-ray lasing.

II. ATOMIC PROCESSES

Illustrated in Fig. 1 are schematic atomic processes along with the associated x-ray emission by inner-shell ionized and hollow atoms. Our method is an extension of the atomic processes model in Refs. [24] and [25]. Namely, we may ignore the other atomic processes, which are treated as slow ones in these references. We consider these processes theoretically and computationally. The photoionization and electron-impact-ionization cross sections (σ^P and σ^e) are derived from the data or the empirical formula in Refs. [29, 30] and [31, 32], respectively. The energy levels, the radiative transition probabilities, and autoionization rates are calculated with the use of Cowan's code [33,34].

The rates of change of concentrations of the various atomic states as illustrated in Fig. 1 may be governed by the following equations:

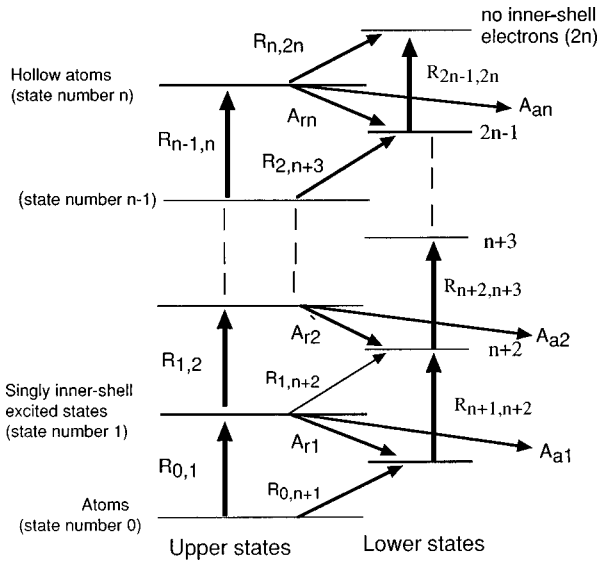

FIG. 1. Atomic processes in x-ray emission from the singly excited states and hollow atoms.

$$\dot{N}_0=-(R_{0,1}+R_{0,n+1})N_0\,,$$

$$\dot{N}_1=R_{0,1}N_0-(A_{r1}+A_{a1}+R_{1,2}+R_{1,n+2})N_1\,,$$

$$\vdots$$

$$\dot{N}_{n-1}=R_{n-2,n-1}N_{n-2}-(A_{rn-1}+A_{an-1}+R_{n-1,n}+R_{n-1,2n-1})N_{n-1}\,,$$

$$\dot{N}_n=R_{n-1,n}N_{n-1}-(A_{rn}+A_{an}+R_{n,2n})N_n\,,$$

$$\dot{N}_{n+1}=R_{0,n+1}N_0+A_{r1}N_1-R_{n+1,n+2}N_{n+1}\,,$$

$$\dot{N}_{n+2}=R_{1,n+2}N_1+A_{r2}N_2+R_{n+1,n+2}N_{n+1}-(A_{rn+1}+A_{an+1}+R_{n+1,n+2})N_{n+1}\,,$$

$$\vdots$$

$$\dot{N}_{2n-1}=R_{n-1,2n-1}N_{n-1}+A_{rn}N_n+R_{2n-2,2n-1}N_{2n-2}-(A_{r2n-1}+A_{a2n-1}+R_{2n-1,2n})N_{2n-1}\,, \qquad (2)$$

with $R_{i,j}=R^e_{i,j}+R^P_{i,j}$, where n is the number of inner-shell electrons. In Na with $2p$ inner-shell electrons ionized, $n=6$ and the subscripts $0,1,\ldots,n,\ n+1,\ldots,2n-1$ correspond to the state of Na atom ($1s^22s^22p^63s$), the upper states for the inner-shell ionization ($1s^22s^22p^53s$), ..., for the hollow atoms ($1s^22s^23s$), and the lower states for the inner-shell ionization ($1s^22s^22p^6$), ..., for the hollow atoms ($1s^22s^22p$), respectively. In the C atoms with $1s$ inner-shell electrons ionized, the subscripts 0, 1, 2, 3, 4 with $n=2$ also represent the initial atoms ($1s^22s^22p^2$), inner-shell excited states ($1s2s^22p^2$), hollow states ($22s^22p^2$), and their lower states ($1s^22s^22p$ and $1s2s^22p$), respectively. The R^P, R^e, A_r, A_a values are the photoionization rate,

electron-impact ionization rate, radiative transition probability, and autoionization rate, respectively. Here R^P and R^e are given by

$$R^P = \int_{E_{I\mathrm{ion}}}^{\infty} \frac{I\sigma^P}{h\nu_I} d(h\nu_I), \tag{3}$$

$$R^e = \int_{E_{e\mathrm{ion}}}^{\infty} v_e \sigma^e n_e dE_e, \tag{4}$$

respectively, where E_e, n_e, I are the electron-impact energy, population of the electrons, and intensity of the source (driving) x rays, respectively. $E_{e\mathrm{ion}}$ and $E_{I\mathrm{ion}}$ are the ionization energy for photoionization and electron-impact ionization, respectively. For the analysis of x-ray laser, the gain Γ of soft x rays from the lasing process by the transition between an upper state and a lower state is given by

$$\Gamma = 2.7\times 10^{-2}\phi_i \frac{P}{g} f_{ul}, \quad \text{with} \quad P = N_{\mathrm{up}} - gN_{\mathrm{low}},$$

$$g = g_{\mathrm{low}}/g_{\mathrm{up}}, \tag{5}$$

where ϕ_i, $N_{\mathrm{up(low)}}$, $g_{\mathrm{up(low)}}$, f_{ul} are the Doppler or Voigt broadening, population, statistical weight of the upper (lower) state, and oscillator strength.

III. X-RAY MEASUREMENT

High-intensity short-pulse x-ray sources commence a new avenue in the x-ray measurement of biology, material matter, and chemistry [11]. In this section, we show that a large population of hollow atoms may be generated by such sources and these hollow atoms have an effect on x-ray measurement method. We take an example of atomic processes of Na for this demonstration.

The N_0 to N_n values in Eq. (2) may be analytically solved as follows:

$$N_0 = N_{00} e^{-(R_{0,1}+R_{0,n+1})t},$$

$$N_1 = \frac{R_{0,1}N_{00}}{R_{0,1}-(R_{1,2}+D_1)}\left(e^{-(R^P_{1,2}+D_1)t} - e^{-(R_{0,1}+R_{0,n+1})t}\right),$$

$$\vdots$$

$$N_k = \left(C_0^k e^{-(R_{0,1}+R_{0,n+1})t} + \sum_{l=1}^{k} C_l^k e^{-(R_{l,l+1}+D_l)t} \right) N_{00} \quad \text{for} \quad k \neq n$$

$$\vdots$$

$$N_n = \left(C_0^n e^{-(R_{0,1}+R_{0,n+1})t} + \sum_{l=1}^{n-1} C_l^n e^{-(R_{l,l+1}+D_l)t} + C_n^n e^{-D_n t} \right) N_{00}, \tag{6}$$

TABLE I. Ionization energies E_{Ion} (in units of eV) of the $3s$ and $2p$ electron, and wavelength of the x-ray laser for the multi-inner-shell excited states of the Na atom.

Ion	E_{Ion} (eV) for $2p$	E_{Ion} (eV) for $3s$	Wavelength (nm)
$1s^2 2s^2 2p^6 3s$	36	5	
$1s^2 2s^2 2p^5 3s$	58	14	39
$1s^2 2s^2 2p^4 3s$	95	25	27
$1s^2 2s^2 2p^3 3s$	110	39	20
$1s^2 2s^2 2p^2 3s$	155	54	15
$1s^2 2s^2 2p 3s$	190	70	12
$1s^2 2s^2 3s$		90	10

with

$$C_0^0 = 1, \quad C_l^k = \prod_{j=l+1}^{k} \frac{R_{j-1,j}}{(R_{j,j+1}+D_j)-(R_{l,l+1}+D_l)} \quad \text{for} \quad l<k$$

$$C_k^k = -\sum_{l=0}^{k-1} C_l^k, \tag{7}$$

$$D_k = A_{rk} + A_{ak} + R_{k,n+k+1},$$

where N_{00} is the population of atoms (0) at $t=0$. The electron-impact ionization rate depends on time. However, the process becomes effective after the electron density is saturated. Namely, we may treat D_k as a time-independent function.

With the use of a usual low intensity x-ray source ($R_{k,k+1} \ll D_k \sim A_{ak}+A_{rk}$), multi-inner-shell ionization processes ($R_{k,k+1}$ for $1 \leq k \leq n-1$) seldom occur because the states can be characterized as

$$e^{-R_{k,k+1}t} \sim 1 \quad \text{and} \quad e^{-D_k t} \sim 0 \tag{8}$$

in Eq. (6) for $1/D_k \ll t \ll 1/R_{k,k+1}$. Namely, from Eq. (6), the N_k values may be given by

$$N_k \sim C_0^k N_{00} \quad \text{with} \quad C_0^0 \sim 1, \quad C_0^k \sim \prod_{j=1}^{k} \frac{R^P_{j-1,j}}{D_j}. \tag{9}$$

The population of multi-inner-shell excited states decreases as the number of inner-shell electrons becomes smaller.

On the other hand, in the high-intensity x-ray measurement where $R^P_{k,k+1} \gg D_k$, Eq. (8) can be rewritten as

$$e^{-R^P_{k,k+1}t} \sim 0 \quad \text{and} \quad e^{-D_k t} \sim 1 \tag{10}$$

for $1/D_k \gg t \gg 1/R^P_{k,k+1}$. The N_k values are given by

$$N_k \sim 0 \quad \text{for} \quad k \neq n,$$
$$N_n \sim C_n^n N_{00} \sim N_{00}. \tag{11}$$

We can find little population of all states except for hollow atoms, that is, the population concentrates in hollow atoms.

Table I lists the ionization energies for the $2p$ electrons and $3s$ electrons, and the wavelength in the $3s \rightarrow 2p$ radia-

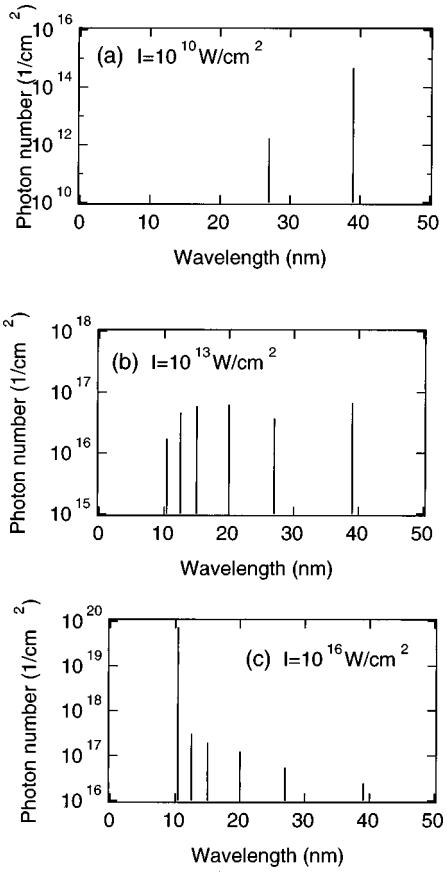

FIG. 2. The total emission from the multi-inner-shell excited states for their wavelength listed in Table I: (a) at $I=10^{10}$, (b) 10^{13}, and (c) 10^{16} W/cm^2.

tive transitions for $1s^22s^22p^63s$, $1s^22s^22p^53s, \ldots,$ $1s^22s^23s$ states of Na. Since the photoabsorption cross sections of $2p$ electrons are much greater than those of $2s$ and $3s$ [29], soft x-ray with broad photon energies may be absorbed mainly along the inner-shell ionization processes of the $2p$ electrons. In the high-intensity x-ray measurement, there are six energy values for the ionization threshold of $2p$ electrons between 30 and 190 eV as is listed in Table I. Furthermore, six values of the wavelength between 10 and 39 nm exist. This means that with use of a high intensity x-ray source, we may have to consider these wavelengths for the fluorescent x-ray analysis, that is, the analysis of x-ray radiation from the multi-inner-shell excited states. This analysis can be applied to a high-Z metal component in low-Z material or molecularity for crystal and biology. For these studies a higher brightness x-ray source is desired for more accurate measurement. Since there is little absorption of soft x rays in hollow (no inner-shell) atoms, high-intensity x rays may be used even for a thick material. (This has been applied only to thin ones because of a lot of absorption through inner-shell excitations or ionizations.)

Figure 2 shows the total photon number given by

$$N_{\text{photon}}=\int_0^{t_{\max}} N_k A_{rk}\,dt \tag{12}$$

for the wavelength of N_k with the intensity values of $I=10^{10}$, 10^{13}, and 10^{16} W/cm^2 and $t_{\max}=800$ fs. N_{photon} from

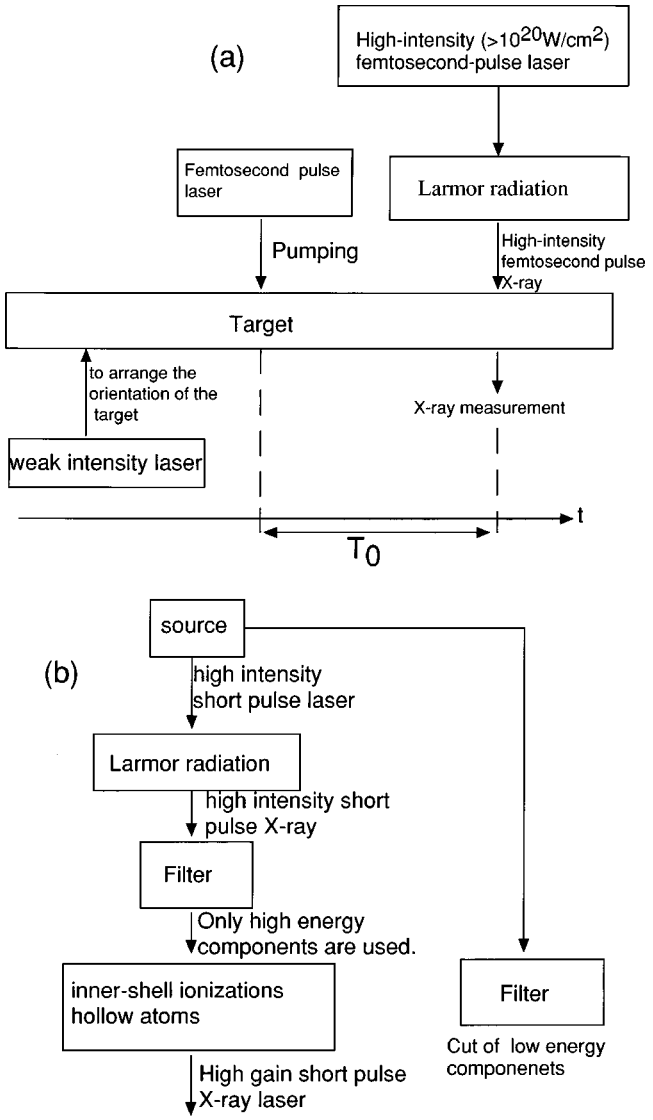

FIG. 3. Our proposal for a class of experiment: (a) x-ray measurement and (b) x-ray laser.

inner-shell excited states remains nearly constant over different I. On the other hand, the N_{photon} from hollow atoms increases very rapidly as I becomes larger. This agrees with Eq. (11). At $I=10^{10}$ W/cm^2 where Eq. (9) is valid, we can see little x-ray emission from hollow atoms, while for $I\sim10^{13}$ ($R^P_{k,k+1}\sim D_k$), and $I\sim10^{16}$ W/cm^2 ($R^P_{k,k+1}\gg D_k$), hollow atom emissions are comparable to and much larger than those of the singly inner-shell excited states, respectively. This means that in the x-ray-absorption measurement and fluorescent x-ray analysis, we cannot ignore the multi-inner-shell excited states for $I\geqslant10^{13}$ W/cm^2.

As mentioned in Sec. I, a high-intensity femtosecond-pulse x-ray source can be applied to the measurement of components, states, structures for femtosecond processes in chemistry and biology. However, even the time resolution of the newest x-ray detector (~2 ps) is useless for such measurement. We propose a class of pump x ray (with a high-intensity femtosecond pulse) probe technology shown in Fig. 3(a). The procedures are as follows. (i) We use weak intensity and long pulse laser in order to arrange the orientation of the target. (ii) The target material is pumped up by a

femtosecond-pulse laser. (iii) After T_0 fs, we execute the high-intensity femtosecond-pulse x-ray measurement such as x-ray diffraction, x-ray absorption, and fluorescent x rays. (iv) Procedures (i)–(iii) are executed for various T_0 values. As a result, we can understand the mechanism as a function of T_0.

IV. X-RAY LASER

A. Proposal of a new class of experiment

Here we suggest a class of x-ray laser experiment by inner-shell ionization and hollow-atom methods. We wish to form a population inversion and to obtain a high gain over a relatively long time, that is, to reduce the population of lower states and to increase that of upper states.

The first key technology in these x-ray laser schemes is pumping by intense broadband x rays with energies of just above the threshold of inner-shell photoionization. At those energies the photoionization cross section for the inner-shell electron is much larger than the other electrons so that population inversion in the inner-shell radiative transition is produced. As is seen from Ref. [29], low-energy photons contribute only to the ionization processes to lower states. Therefore, we suggest that only high-energy photons should be employed by eliminating low-energy photons with the use of a filter. The photon energy considered here are $E_p \geqslant 40$ eV for Na and $E \geqslant 300$ eV for C, respectively.

However, in the previous studies, electron-impact ionization, which follows inner-shell photoionization, is considered to have a detrimental effect on x-ray lasing [22–26]. In the case of a C laser, electron-impact ionization from a neutral C atom directly causes an increase in the lower laser level $(1s^2 2s^2 2p)$. The electron-impact ionization R^e is a function of the electron density n_e and electron-impact ionization rate coefficient $\langle v_e \sigma^e \rangle$ [see Eq. (4)]. n_e and $\langle v_e \sigma^e \rangle$ are approximately proportional to t and inversely proportional to v_e, respectively. Therefore, t (v_e) should be as short (fast) as possible. To reduce t, we suggest the use of a high-intensity short-pulse pumping source because it can make all the initial atoms ionize in a moment. This idea leads to the hollow atom method discussed in Sec. IV C.

In the presence of ultrafast high-intensity x rays as a pump source, successive inner-shell photoionization of an inner-shell ionized ion takes place until all electrons in the shell are removed to produce hollow atoms, before those states are destroyed through various decay processes including electron-impact ionization and autoionization. Surprisingly, the atomic kinetics could even become simpler if a large fraction of initial atoms are ionized up to a hollow-atom state. This leads to large gain in the inner-shell radiative transition. Moreover, as the population of the lower level of x-ray lasers such as $1s^2 2s^2 2p$ could also be removed, that gain could be sustained much longer in this scheme. Using these ultrafast atomic processes, we suggest significant improvement of gain of photopump x-ray lasers in Sec. IV C.

Figure 3(b) shows our proposal of a class of experiments. Via the mechanism of the Larmor radiation resulting from the irradiation of a high-intensity ($\geqslant 10^{20}$ W/cm^2) short-pulse laser on a plasma, x rays with high intensity and short pulse are emitted [5]. With the use of an appropriate filter, only x rays with high-energy photons can be selected. As soon as the pumping x rays interact with Na or C, the lasing of x rays by inner-shell ionization or hollow-atom methods may be achieved. Another filter may be employed in order to avoid the interaction of the short pulse laser on atoms because it may destroy the inner-shell excited states and hollow atoms by the optical field ionization process.

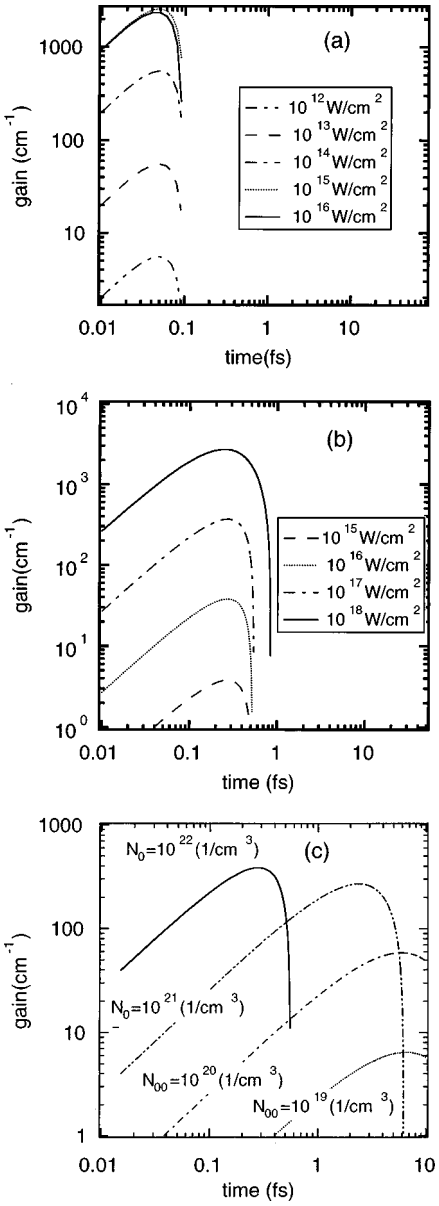

FIG. 4. Gain (cm^{-1}) vs time (fs) for the conventional inner-shell method; (a) Na and (b) C. Inset shows the x-ray intensity value for each curve. (c) Same as Fig. 4(b) for $I = 10^{17}$ W/cm^2: Density values are indicated on each curve.

B. Inner-shell ionization method

In the conventional inner-shell ionization method, the radiative transitions of $1s^2 2s^2 2p^5 3s \rightarrow 1s^2 2s^2 2p^6$ of Na atom and $1s 2s^2 2p^2 \rightarrow 1s^2 2s^2 2p$ of C atom may be employed for x-ray laser emission. The wavelengths considered here are about 40 nm for Na and 4 nm for C, respectively. The N_i values can be expanded in terms of low-order processes because of a short time duration (see Fig. 4). Then the popula-

tions of the upper (N_1) and lower (N_{n+1}) states can be obtained as [26]

$$N_1 \sim R^P_{0,1} N_{00}\{t-(R^P_{0,1}+R^P_{1,2})t^2/2\}, \tag{13}$$

$$N_{n+1} \sim \langle v_e \sigma^e_{0,n+1}\rangle R^P_{0,1} N^2_{00} t^2/2, \tag{14}$$

where n_e can be the population of electrons ejected mainly from Na atom through the inner-shell photoionization process. Therefore, we can set

$$n_e \sim \sum_i N_i \sim N_1. \tag{15}$$

The population inversion P in Eq. (5) becomes:

$$P = R^P_{0,1} N_{00}[t-(R^P_{0,1}+R^P_{1,2}+g\langle v_e \sigma^e_{0,n+1}\rangle N_{00})t^2/2], \tag{16}$$

where only the fast processes such as $R^P_{0,1}$, $R^P_{1,2}$, and $g\langle v_e \sigma^e_{0,n+1}\rangle$ are considered. The maximum value of P and its time rate of change are given by

$$P_{\max} = \frac{R^P_{0,1} N_{00}}{2(R^P_{0,1}+R^P_{1,2}+g\langle v_e \sigma^e_{0,n+1}\rangle N_{00})} = \frac{\sigma^P_{0,1} I N_{00}}{\{2(\sigma^P_{0,1}+\sigma^P_{1,2})I + g\langle v_e \sigma^e_{0,n+1}\rangle N_{00} h\nu_I\}}, \tag{17}$$

$$t_{\max} = \{R^P_{0,1}+R^P_{1,2}+g\langle v_e \sigma^e_{0,n+1}\rangle N_{00}\}^{-1}. \tag{18}$$

From Eqs. (17) and (18), we see that in the case of $R_{0,1} \sim g\langle v_e \sigma^e_{0,n+1}\rangle$, the $P_{\max}$ value is saturated. Then, the saturated intensity ($I_{\rm sat}$) and the saturated initial density ($N_{00,\rm sat}$) are obtained as

$$I_{\rm sat} = \frac{h\nu_I g\langle v_e \sigma^e_{0,n+1}\rangle N_{00}}{\sigma^P_{0,1}+\sigma^P_{1,2}}, \quad P_{\max,{\rm sat},I} = \frac{N_{00}\sigma^P_{0,1}}{2(\sigma^P_{0,1}+\sigma^P_{1,2})}, \tag{19}$$

$$N_{00,\rm sat} = \frac{2(\sigma^P_{0,1} I + \sigma^P_{1,2} I)}{g\langle v_e \sigma^e_{0,n+1}\rangle h\nu_I}, \quad P_{\max,{\rm sat},N} = \frac{I\sigma^P_{0,1}}{g\langle v_e \sigma^e_{0,n+1}\rangle h\nu_I}. \tag{20}$$

Here $P_{\max,{\rm sat},I}$ and $P_{\max,{\rm sat},N}$ are the $P_{\max}$ values at the saturation of I and that of N_{00}, respectively. For C, at $E_p \sim 600$ eV, $g\langle v_e \sigma^e_{0,3}\rangle N_{00} \sim 10^{14}$/s and $\sigma^P_{0,1} \sim \sigma^P_{1,2} \sim 10^{-19}$ cm^2. On the other hand, for Na, at $E_p = 100$ eV, $g\langle v_e \sigma^e_{0,7}\rangle N_{00} \sim 10^{14}$/s and $\sigma^P_{0,1} \sim \sigma^P_{1,2} \sim 10^{-17}$ cm^2. Therefore, $I_{\rm sat}$ are greater than 10^{16} W/cm^2 for C and 10^{14} W/cm^2 for Na, respectively.

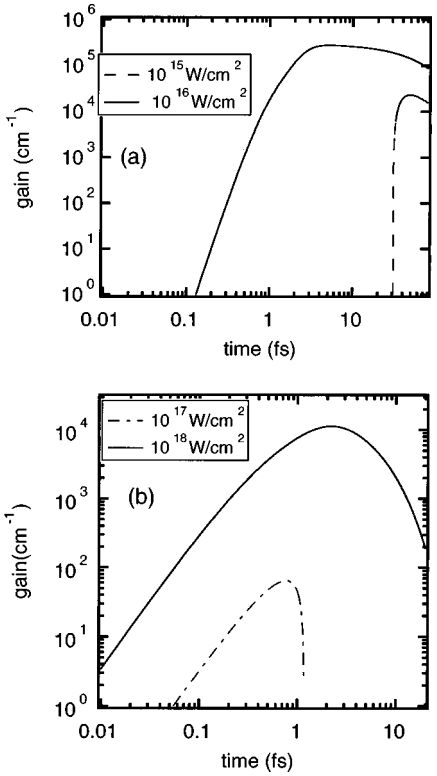

FIG. 5. The same as Fig. 4 for the hollow-atom method.

C. Hollow-atom method

Here the x-ray radiative transition process is the transition of $1s^2 2s^2 3s \rightarrow 1s^2 2s^2 2p$ with the wavelength of 10 nm for Na or that of $2s^2 2p^2 \rightarrow 1s 2s^2 2p$ with that of 3.5 nm for C. We find that a large gain can be obtained for the x-ray laser from hollow atoms resulting from the ultrafast inner-shell ionization process: (i) a large population of the upper state, and (ii) a positive value for the inversion population [$P>0$ in Eq. (5)]. In this process ($R^P_{l,l+1} \gg D_l$ for $l \leqslant n-1$), only the photo inner-shell ionization rate ($R^P_{l,l+1}$) needs to be treated. The population of lower states can be ignored. The populations of upper states $N_0 \sim N_n$ may be obtained by Eq. (11). Therefore, a large population of hollow atoms is realized during $1/R^P_{l,l+1} \ll t \sim 1/(R^e + A_r + R^P_{l,2l-1})$. (This condition can be attained for $I \geqslant 10^{16}$ W/cm^2 for Na and $I \geqslant 10^{18}$ W/cm^2 for C, respectively.)

The intensity $I \geqslant 10^{18}$ W/cm^2 of lasing with C agrees well with our simulation, which will be discussed later. On the other hand, in the case of Na, simulation shows that a large gain x-ray lasing from hollow atoms can take place even when the pumping x-ray source intensity is at $I = 10^{15}$ W/cm^2 [see Fig. 5(a)]. This arises from the fact that the lifetime of the upper states (N_n) is much longer than that of the lower states (N_{2n-1}). Namely, for the use of the source with $I = 10^{15}$ W/cm^2 and $E_p = 50$–500 eV, $A_{rn} + R^P_{n,2n-1} < R^e_{n,2n}$ ($\sim 10^{13}$ s^{-1}) $\ll R^P_{2n-1,2n}$ ($\sim 10^{14}$ s^{-1}), though $R^e_{0,n+1} \sim R^P_{0,1}$. The R^e values are controlled by the photon energy (E_p) distribution of the x-ray source because the electron-impact ionization cross sections are a function of $E_e (= E_p - E_{I\rm ion})$ only for $E_e > E_{e\rm ion}$. Choosing an optimal distribution of the pump x-ray source photon energy, we may

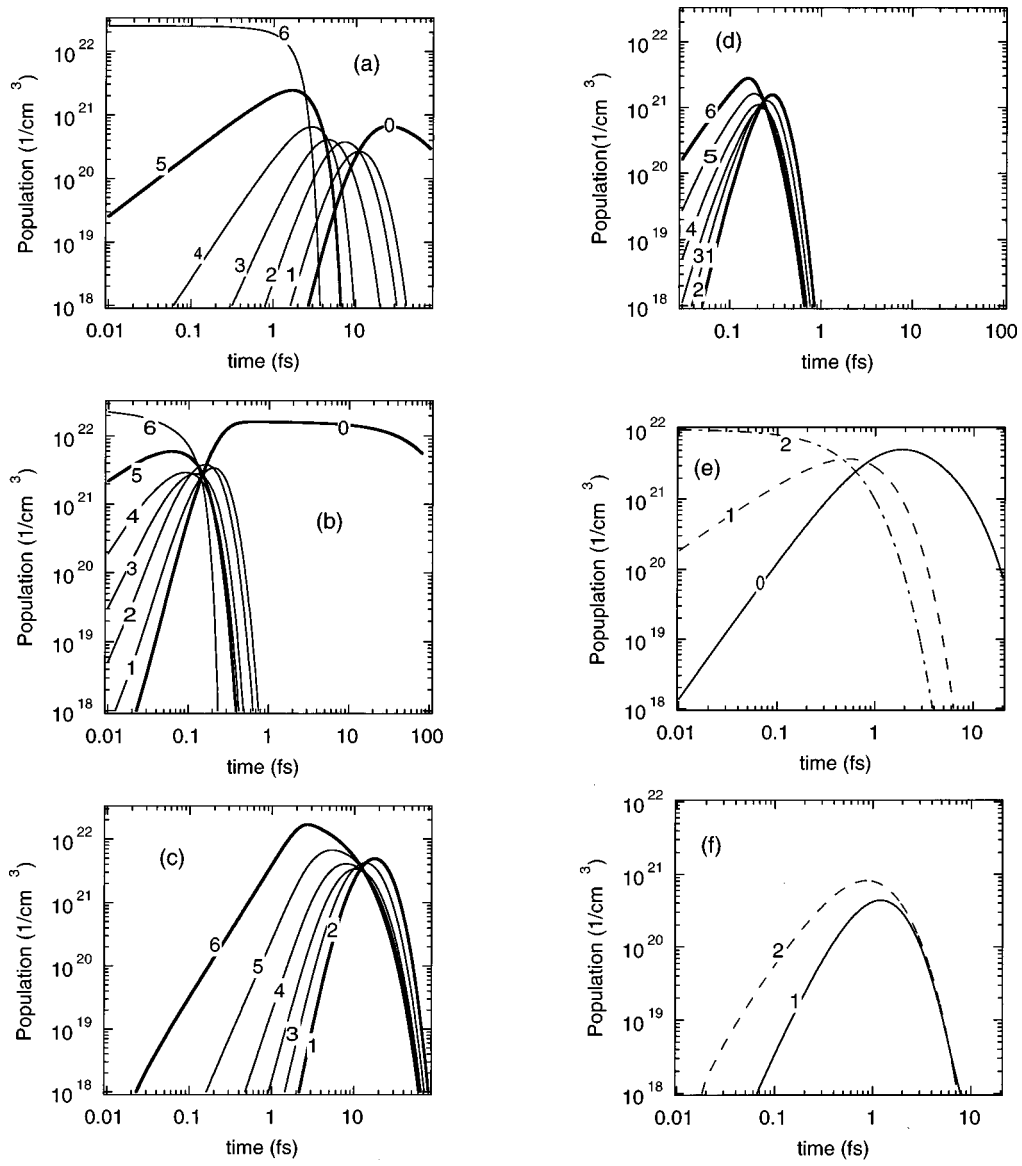

FIG. 6. Population (1/cm^3) vs time (fs); upper states with (a) $I=10^{15}$ and (b) $I=10^{17}$ W/cm^2, and lower states with (c) $I=10^{15}$ and (d) $I=10^{17}$ W/cm^2 of the Na atoms; the lines express the number of $2p$ electrons. (e) Upper states and (f) lower states of C atoms for $I=10^{18}$ W/cm^2; the lines express the number of $1s$ electrons.

be able to further reduce the necessary intensity of pump x rays from $I=10^{15}$ W/cm^2.

In the case of C, the population of the upper state (N_2) and the lower state (N_4) for hollow atoms can be expanded to yield

$$N_2 \sim R_{0,1}R_{1,2}N_{00}(t^2/2 - A_{a3}t^3/6), \tag{21}$$

$$N_4 \sim R_{0,1}R_{3,4}\langle v_e\sigma^e_{0,3}\rangle N_{00}^2 t^3/3 - \frac{1}{12}R_{3,4}R_{0,1}\langle v_e\sigma^e_{0,3}\rangle N_{00}^2(R_{0,1}+R_{1,2}+R_{3,4}+R_{4,6})t^4. \tag{22}$$

The second- to fourth-order processes play an important role, as is illustrated in Fig. 1. Then, P in Eq. (5) is evaluated as

$$P = N_2 - gN_4 \sim \frac{1}{12}R_{3,4}R_{0,1}g\langle v_e\sigma^e_{0,3}\rangle \times N_{00}(R_{0,1}+R_{1,2}+R_{3,4}+R_{4,6})t^2 \times \left(t - \frac{2}{R_{0,1}+R_{1,2}+R_{3,4}+R_{4,6}}\right)^2 + R_{0,1}R_{1,2}N_{00}t^2/2 - g\langle v_e\sigma^e_{0,3}\rangle R_{3,4}R_{0,1}N_{00}^2 \frac{1}{R_{0,1}+R_{1,2}+R_{3,4}+R_{4,6}}t^2/3. \tag{23}$$

Here we consider only the $R_{l,l+1}$ because of $R^P_{l,l+1} \gg D_l$ for $l \leqslant n-1$. Further, we find that the lasing condition is determined by the following relationship:

$$R^P_{1,2cr} \sim \tfrac{1}{6}\, g\langle v_e\sigma^e_{0,3}\rangle N_{00}, \tag{24}$$

This condition can be cast in the critical x-ray intensity I_{cr} above which the lasing does occur:

$$I_{cr} \sim \frac{1}{6} \frac{g\langle v_e \sigma^e_{0,3} \rangle N_{00} h\nu}{\sigma^P_{1,2}}. \tag{25}$$

At $E_p = 600$ eV and $N_{00} = 10^{22}$ cm^{-3}, $g\langle v_e \sigma^e_{0,3} \rangle N_{00} \sim 2 \times 10^{15}$ s^{-1} and $\sigma^P_{1,2} \sim 10^{-19}$ cm^2. Therefore, I_{cr} is greater than 2×10^{17} W/cm^2 for the C system.

The following properties are noted for the hollow-atom method (in comparison with the conventional inner-shell ionization method). (1) A much larger population of the upper states can be obtained [see Eq. (11)]. (2) The lower states decay much more rapidly because of the ultrafast inner-shell ionization process: The effect of secondary electron-impact ionization process may be ignored. (3) With the use of high initial density of atom ($\sim 10^{22}$ cm^{-3}), high-gain x-ray laser emission occurs for a longer time. This arises from properties (1) and (2). (4) The wavelength becomes shorter than the inner-shell ionization method (see Table I). (5) The Na atomic process may be present in a molecular NaH crystal. (6) Little x-ray absorption is found because of no inner-shell electrons. (7) A high intensity x-ray source with broad photoenergy is needed.

D. Simulations

The physical process analytically outlined above is now illuminated with computer simulation. In the simulation all the processes in Fig. 1 are considered. Figures 4(a) and 4(b) show the gain Γ as a function of time for the conventional inner-shell ionization method in Na and C, respectively. The x-ray sources with $I \geqslant 10^{13}$ and 10^{16} W/cm^2 are required to produce Γ of about 10 cm^{-1} for Na and C at the density of $\sim 10^{22}$ cm^{-3}, respectively. However, both duration times of large gain are shorter than 1 fs. (This feature may be useful as an ultrashort pulse x-ray laser.) In order to obtain a longer duration time (>10 fs), the density of initial atoms needs to be decreased to as little as 10^{20} cm^{-3}, as mentioned in Refs. [23–25]. Then, as seen in Fig. 4(c), only a (relatively) low gain can be achieved. Our hollow-atom method can achieve a large gain over a relatively long time.

Figures 5(a) and 5(b) show the gain for the hollow-atom method corresponding to Figs. 4(a) and 4(b), respectively. From Fig. 5, we find that the x-ray laser from hollow atoms is realized for $I \geqslant 10^{15}$ W/cm^2 in Na and $I \geqslant 10^{18}$ W/cm^2 in C. (We should choose the best atoms as a target matter in compliance with the purpose.) The gain Γ is greater than 10^4 cm^{-1}, and moreover, the duration time is much longer than that in Figs. 4(a) and 4(b). The time is determined by the Auger rate (~ 10 fs) for C and by the electron-impact ionization process (~ 100 fs) for Na.

Figures 6(a) and 6(b) show the populations of the initial atoms, various inner-shell excited states, and hollow atoms of Na at $I = 10^{15}$ W/cm^2 and 10^{17} W/cm^2, respectively. The populations of hollow atoms are about 4% at $I = 10^{15}$ W/cm^2 and 60% at 10^{17} W/cm^2 of the initial Na atoms. Namely, the relationship (11) is valid for $I \geqslant 10^{17}$ W/cm^2. Figures 6(c) and 6(d) show the populations of the $1s^2 2s^2 2p^6$ (the lower state for inner-shell excited $1s^2 2s^2 2p^5 3s$ state), . . . , and $1s^2 2s^2 2p$ (the lower state for hollow atoms $1s^2 2s^2 3s$) at $I = 10^{15}$ W/cm^2 and 10^{17} W/cm^2, respectively. In Fig. 6 all of the populations decay rapidly except for that of hollow atoms because of the ultrafast inner-shell ionization process [see Eq. (11)]. As a result, the x-ray laser with a gain of more than 10^4 cm^{-1} continues to be sustained during the lifetime of hollow atoms. In contrast with the conventional self-terminating inner-shell ionization lasing, our hollow-atom method is attractive for the x-ray laser emission. The population of lower states rapidly diminishes. Figures. 6(e) and 6(f) appear similar to Figs. 6(a) and 6(c) for C at $I = 10^{18}$ W/cm^2, respectively. The same trends as those in Figs. 6(a)–6(d) are seen.

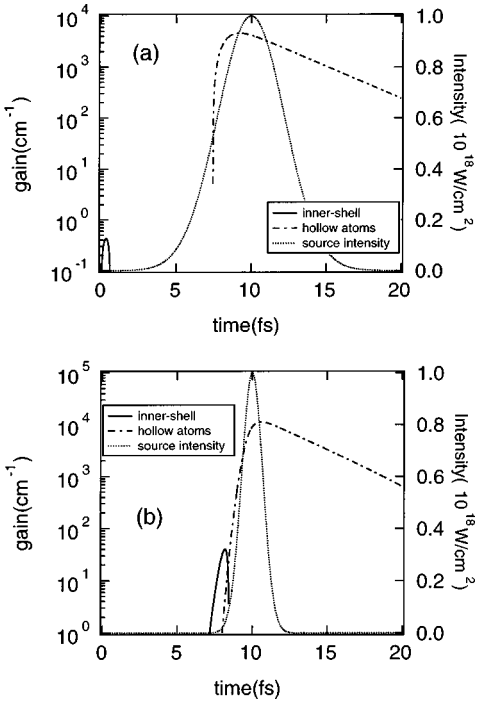

FIG. 7. Gain (cm^{-1}) vs time (fs) for the inner-shell ionization method and the hollow-atom method. Time dependent function for the source is shown.

Figure 7 shows Γ with the use of a time-dependent x-ray pumping source from inner-shell excited states and hollow atoms of C. The time-dependent intensity of the source is given by

$$I(t) = I_0 \exp[-a(t - t_{peak})^2] \tag{26}$$

with $I_0 = 10^{18}$ W/cm^2, $t_{peak} = 10$ fs, and $a = 0.05$ [Fig. 7(a)], 0.1 [Fig. 7(b)]. For the inner-shell ionization method, we should employ a source with weak time dependence. On the other hand, in the hollow-atom method the time dependence of the source matters little. This is due to the difference in the decay rates of the lower states. Little decay exists in the inner-shell ionization method, while fast decay processes are present in the hollow-atom method.

V. SUMMARY

We have modeled the ultrafast atomic process with the use of a high-intensity short-pulse x-ray pumping source relevant for x-ray lasing of Na and C. This atomic process leads to the x-ray laser emission from hollow atoms. This method

has a clear advantage over the conventional inner-shell ionization method as follows. The lower state decays much more rapidly and a much larger population of the upper states can be obtained. A high gain continues to be sustained for a longer time. The hollow-atom process allows shorter wavelengths of the x-ray laser than those in the conventional inner-shell ionization method: Further, the longer lifetime of the upper states by electron-impact ionization is sustained. A NaH crystal may be employed to the advantage of the Na process. For both inner-shell ionization and hollow-atom methods, the x-ray laser with a $3s \rightarrow 2p$ transition of Na requires a much smaller intensity x-ray pumping source than that with $2p \rightarrow 1s$ of C. It should be noted that the choice of target atoms may be the key to these x-ray laser sources. We pointed out that hollow atoms may play an important role in high-brightness x-ray measurement of ultrafast processes in chemistry, biochemistry, biology, and materials. We also suggest classes of experiments of pump high-intensity femtosecond-pulse x-ray measurement and x-ray lasers.

ACKNOWLEDGMENTS

We wish to thank Dr. T. Kato (NIFS), Dr. Y. Ueshima, Dr. N. Ichinose, and Dr. J. Chihara (JAERI) for their useful discussions. R. D. Cowan's code is employed for the atomic structures. T.T. is supported in part by the NSF and the U.S. DOE.

[1] P. Gibbon, Phys. Rev. Lett. **76**, 50 (1996).
[2] J. J. Macklln, J. D. Kmetec, and C. L. Gordon, Phys. Rev. Lett. **70**, 766 (1993).
[3] T. D. Donnelly, T. Ditmire, K. Neuman, M. D. Perry, and R. W. Falcone, Phys. Rev. Lett. **76**, 2472 (1996).
[4] J. D. Kmetec, C. L. Gordon III, J. J. Macklin, B. E. Lemoff, G. S. Brown, and S. E. Harris, Phys. Rev. Lett. **68**, 1527 (1992).
[5] Y. Ueshima, Y. Kishimoto, A. Sasaki, Y. Sentoku, and T. Tajima, in *Proceedings of the First JAERI-Kansai International Workshop on Ultrashort-Pulse Ultrahigh-Power Lasers and Simulation for Laser-Plasma Interactions, Kyoto, Japan, 1997* (JAERI, Tokai, 1997), Vol. 98-004, p. 31.
[6] M. D. Perry and G. Mourou, Science **264**, 917 (1994).
[7] C. P. J. Barty, Laser Focus World **32**, 93 (1996).
[8] C. P. J. Barty, T. Guo, C. Le Blanc, F. Raksi, C. Rose-Petruck, J. A. Squier, K. R. Wilson, V. V. Yakovlev, and K. Yamakawa, Proc. SPIE **2701**, 84 (1996).
[9] K. Yamakawa, T. Guo, G. Korn, C. Le Blanc, F. Raksi, C. Rose-Petruck, J. A. Squier, V. V. Yakovlev, and C. P. J. Barty, Proc. SPIE **2701**, 198 (1996).
[10] F. Brunel, Phys. Rev. Lett. **59**, 52 (1987).
[11] T. Guo, C. Rose-Petruck, R. Jimenez, F. Raksi, J. Squier, B. Walker, K. R. Wilson, and C. P. J. Barty (unpublished).
[12] G. R. Fleming, *Chemical Applications of Ultrafast Spectroscopy* (Oxford University Press, New York, 1996).
[13] R. W. Schoenlein, L. A. Peteanu, R. A. Mathies, and C. V. Shank, Science **254**, 412 (1991).
[14] M. H. Vos, F. Rappaport, J.-C. Lambry, J. Breton, and J.-L. Martin, Nature (London) **363**, 320 (1993).
[15] H. Kandori, H. Sasabe, K. Nakanishi, T. Yoshizawa, T. Mizukami, and Y. Shichida, J. Am. Chem. Soc. **118**, 1002 (1996).
[16] P. O. Andersson, R. J. Cogdell, and T. Gillbro, Chem. Phys. **210**, 195 (1996).
[17] M. Ricci, S. E. Bradforth, R. Jimenez, and G. R. Fleming, Chem. Phys. Lett. **259**, 381 (1996).
[18] S. Akimoto, S. Takaichi, T. Ogata, Y. Nishimura, I. Yamazaki, and M. Mimuro, Chem. Phys. Lett. **260**, 147 (1996).
[19] J. P. Briand, B. d'Etat, D. Schneider, M. Clark, and V. Decaux, Nucl. Instrum. Methods Phys. Res. B **87**, 138 (1994).
[20] Y. Yamazaki, S. Ninomiya, F. Koike, H. Masuda, T. Azuma, K.-I. Komaki, K. Kuroki, and M. Sekiguchi, J. Phys. Soc. Jpn. **65**, 1192 (1996).
[21] J. P. Briand, B. d'Etat, D. Schneider, M. A. Briere, V. Decaux, J. W. McDonald, and S. Bardin, Phys. Rev. A **53**, 2194 (1996).
[22] M. A. Duguay and M. Rentzepis, Appl. Phys. Lett. **10**, 350 (1967).
[23] T. S. Axelrod, Phys. Rev. A **13**, 376 (1976).
[24] H. C. Kapteyn, Appl. Opt. **31**, 4391 (1992).
[25] S. J. Moon, D. C. Eder, and G. L. Strobel, in *X-Ray Lasers 1994*, edited by David C. Elder and Dennis L. Matthews, AIP Conf. Proc. No. **332** (American Institute of Physics, New York, 1994), p. 262.
[26] G. L. Strobet, D. C. Eder, and P. Amendt, Appl. Phys. B: Lasers Opt. **B58**, 45 (1994).
[27] K. Moribayashi, A. Sasaki, Y. Ueshima, and T. Tajima (unpublished).
[28] J. Chihara (private communications).
[29] J. J. Yeh and I. Lindau, At. Data Nucl. Data Tables **32**, 1 (1985).
[30] Y. B. Zel'dovich and Y. P. Raizer, *Physics of Shock Waves and High Temperature Hydrodynamic Phenomena* (Academic, New York, 1966), p. 265.
[31] W. Lotz, Z. Phys. **232**, 101 (1970).
[32] L. B. Golden and D. H. Sampson, J. Phys. B **10**, 2229 (1977).
[33] R. D. Cowan, J. Opt. Soc. Am. **58**, 808 (1968).
[34] R. D. Cowan, *The Theory of Atomic Structure and Spectra* (University of California Press, Berkeley, 1981).